

STAGNATION POINT HEATING OF BLUNT BODIES IN LOW-DENSITY HYPERSONIC FLOW

Wilson F. N. Santos
 Combustion and Propulsion Laboratory
 National Institute for Space Research
 Cachoeira Paulista, SP 12630-000 Brazil

ABSTRACT

A numerical study is reported on power law shaped leading edges situated in a rarefied hypersonic flow. The sensitivity of the heat flux and drag coefficient to shape variations of such leading edges is calculated by using a Direct Simulation Monte Carlo method. Calculations show that the stagnation point heating on power law leading edges with finite radius of curvature follows the same relation for classical blunt body in continuum flow; it scales inversely with the square root of the curvature radius. Furthermore, for those leading edges with zero or infinity radii of curvature, the heat transfer behavior is in surprising agreement with that for classical blunt body far from the nose of the leading edges.

NOMENCLATURE

A	constant in power-law body equation	s	arc length, m
c'	thermal velocity of the molecule, m/s	T	temperature, K
C_d	drag coefficient, $2F/\rho_\infty V_\infty^2 H$	V	velocity, m/s
C_h	heat transfer coefficient, $2q_w/\rho_\infty V_\infty^3$	x	cartesian axis in physical space
e	energy, J	y	cartesian axis in physical space
F	drag force, N	η	coordinate normal to body surface
H	body height at the base, m	ξ	coordinate tangent to body surface
Kn	Knudsen number	λ	mean free path, m
L	body length, m	ρ	density, kg/m^3
m	mass, kg	θ	wedge half angle, body slope angle, deg
M	Mach number		
n	body power law exponent	Subscript	
q	heat flux, W/m^2	i	refers to incident molecule
R	circular cylinder radius, m	r	refers to reflect molecule
R_c	radius of curvature, m	w	wall conditions
R_n	nose radius, m	∞	freestream conditions
Re	Reynolds number		

INTRODUCTION

For flight at hypersonic speeds, dissociation and ionization of the air may have a considered effect on the aerodynamic characteristics of a body. As aerodynamic heating may cause serious problems at these speeds, the removal of heat near the front of the body must be considered. Since the stagnation region is the most thermally stressed zone, this particular region is of considerable practical as well as theoretical

interest. For this purpose, the vehicle leading edges must be sufficiently blunt in order to reduce the heat transfer rate to acceptable levels, and possibly to allow for internal heat conduction. The use of blunt-nosed shapes tends to alleviate the aerodynamic heating problem since the heat flux for blunt bodies scales inversely with the square root of the nose radius. In addition, the reduction in heating rate for a blunt body is accompanied by an increase in heat capacity, due to the increased volume. However, designing a hypersonic vehicle leading edge involves a tradeoff between making the leading edge sharp enough to obtain acceptable aerodynamic and propulsion efficiency and blunt enough to reduce the aerodynamic heating in the stagnation region.

Mason and Lee [1] have demonstrated that some geometrically blunt configurations may actually behave as if they were aerodynamically sharp. Power law shapes ($y \sim x^n$, $0 < n < 1$) were shown to have an infinite body slope at the nose and yet have zero radius of curvature at the nose for certain values of power law exponent n . Their analysis describes the details of the geometry and aerodynamics of low-drag axisymmetric bodies by using Newtonian theory. However, one of the important aspects of the problem, stagnation point heat transfer, was not considered.

A number of theoretical and numerical predictions of stagnation point heat transfer on blunt bodies has been reported in the literature [2-10]. The work of Fay and Riddell [5] is the reference point for the scientists working on aerodynamic heating. Due to their simplicity, the Fay-Riddell correlation formulas are still in use today for the thermal analysis of hypersonic vehicles.

Theoretical formulations, experimental data, and semi-empirical formulas [10] all agree in the fact that stagnation point heat transfer for blunt body in continuum flow is inversely proportional to the square root of the nose radius of the leading edge, i.e.,

$$q \propto \frac{1}{\sqrt{R_n}} \quad (1)$$

In addition to the shape of the body, the stagnation point heat transfer is dependent on Mach number, Reynolds number and Knudsen number.

The purpose of this paper is to investigate the effect of the power law exponent on the heat transfer to the body surface and the drag acting on the surface of such leading edges. Attention will be addressed to the heat transfer behavior in comparison to the Eq. (1), since the radius of curvature for such shapes goes to zero or infinity for certain power law exponents.

The flow conditions represent those experienced by a spacecraft at altitude of 70 km. This altitude is associated with the transitional regime that is characterized by the Knudsen number Kn of the order of 10^{-2} or larger. Therefore, the focus of the present study is the low-density region in the upper atmosphere, where numerical gaskinetic procedures are available to simulate hypersonic flows. High-speed flows under low-density conditions deviate from a perfect gas behavior because of the excitation of rotation, vibration and dissociation. At high altitudes, and therefore low density, the molecular collision rate is low and the energy exchange occurs under nonequilibrium conditions. In such a circumstance, the degree of molecular nonequilibrium is such that the Navier-Stokes equations are inappropriate. For the simulation of such complicated flow phenomena, models and assumptions that must be checked separately are necessary. In the current study, Direct Simulation Monte Carlo method is used to calculate the rarefied hypersonic two-dimensional flow.

LEADING-EDGE GEOMETRY DEFINITION

In dimensional form, the body power law shapes are given by the following expression,

$$y = Ax^n \quad (2)$$

where n is the power law exponent and A is the power law constant, which is a function of n .

The radius of curvature R_c for the shapes defined by Eq. (2), obtained from the general formula for the longitudinal radius of curvature, is as follows,

$$R_c(x) = \frac{1}{|nA(n-1)|} \left[x^{\frac{2(2-n)}{3}} + (nA)^2 x^{\frac{2(2n-1)}{3}} \right]^{\frac{3}{2}} \quad (3)$$

By taking the limit of Eq. (3) as $x \rightarrow 0$, one obtains the value of the radius of curvature at the nose of the leading edge. The first term in the square bracket vanishes for $n \geq 2$, a range of not practical interest. The exponent of the second term in the bracket controls the result for practical cases. For values of $0 < n < 1$, the nose radius goes to infinite for $n < 1/2$, it is finite and equal to $A^2/2$ for $n = 1/2$ and goes to zero for $n > 1/2$. Therefore, only one value of n produces a nonzero finite value for the leading-edge radius.

The power-law shapes are modeled by assuming a sharp leading edge of half angle θ with a circular cylinder of radius R inscribed tangent to this wedge. The power law shapes, inscribed between the wedge and the cylinder, are also tangent to the wedge and the circular cylinder at the same common point where they have the same slope angle. It is assumed that the wedge half angle is 10 deg, the circular cylinder diameter of 10^{-2} m and power law exponents of $1/4$, $1/2$ and $3/4$, which yield infinite, finite and zero for the radius of curvature, respectively. Figure 1 illustrates schematically this construction for this set of power law leading edges.

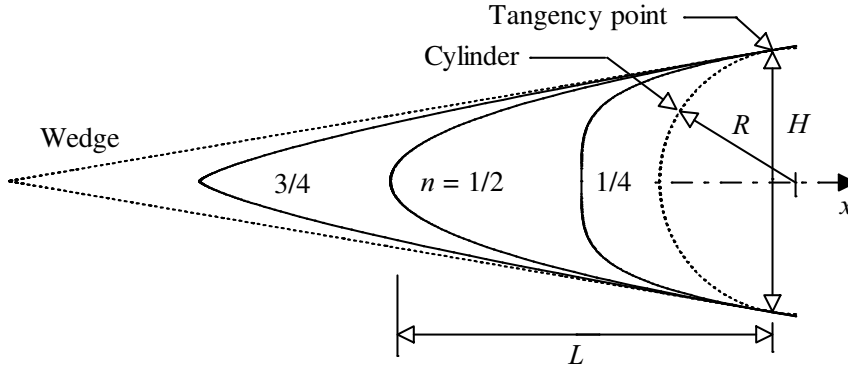


Figure 1: Drawing illustrating the leading edge geometry.

From geometric considerations, the power law constant A is obtained by matching slope on the wedge, circular cylinder and power law body at the tangency point. The common body height H at the tangency point is equal to $2R \cos \theta$. In this way, for the power law shapes to be investigated in this work, the power law constant A and the body length L from the nose to the tangency point are listed in Table 1.

Table 1: Characteristics dimensions of the power law shapes

Exponent n	$A[m^{1-n}]$	$L[m]$	L/H
1/4	1.70348×10^{-2}	7.84964×10^{-3}	0.774
1/2	4.16711×10^{-2}	1.39628×10^{-2}	1.418
3/4	8.94383×10^{-2}	2.09442×10^{-2}	2.127

A geometrically blunt body is defined to be one with a slope ($dy/dx = \infty$) at the tip that corresponds to an angle of 90 deg. On the other hand, a geometrically sharp body is defined to be one with a finite slope ($dy/dx \neq \infty$) at the tip, and the leading-edge radius is zero. The body slope angles at the nose ($x = 0$) for

power law shapes are 90 deg for values of $0 < n < 1$. Moreover, the radius of curvature changes from zero to infinity at the same range of n . Therefore, the power law shapes are blunt even though some of them have a zero nose radius. As a result, some power law shapes exhibit both blunt and sharp geometric properties.

COMPUTATIONAL METHOD AND PROCEDURE

A number of significant problems in fluid mechanics involve transitional flows, i.e., flows for which the mean free path is of the same order of magnitude as a characteristic dimension. The most successful numerical technique for modeling complex transitional flows has been the Direct Simulation Monte Carlo (DSMC) method [11]. It has been recognized as an extremely powerful technique capable of predicting an almost unlimited variety of rarefied flowfields in the regimes where neither the Navier-Stokes nor the free molecular approaches are appropriate. The DSMC method treats transitional flows on a molecular basis, statistically representing a real gas by thousands or millions of simulated molecules. The positions, velocities, and initial state of these simulated molecules are stored and modified in time in the process of molecules moving, colliding among themselves, and interacting with boundaries in simulated physical space. The simulation time of the DSMC method is a real physical time and all DSMC calculations are treated as unsteady state. The solution of the steady-state case is the asymptotic limit of the unsteady flow.

In this study, the molecular collisions are modeled using the variable hard sphere (VHS) molecular model [12]. In this model, the temperature dependency of the viscosity is considered by a variable cross section that is inversely proportional to the relative collision energy between the colliding molecules. The energy exchange between kinetic and internal modes is controlled by Borgnakke-Larsen statistical model [13]. The essential feature of this model is that a part of collisions is treated as completely inelastic. Simulations are performed using air as working fluid with two chemical species, N_2 and O_2 . Energy exchanges between the translational and internal modes are considered. The vibrational temperature is controlled by the distribution of energy between the translational and rotational modes after an inelastic collision. The probability of an inelastic collision determines the rate at which energy is transferred between the translational and internal modes after an inelastic collision. For a given collision, the probabilities are designated by the inverse of the relaxation numbers, which correspond to the number of collisions necessary, on average, for a molecule to relax. The relaxation numbers are traditionally given as constants, 5 for rotation and 50 for vibration. Diffuse reflection with full thermal accommodation is assumed for the gas-surface interaction modeling. In this model, the reflection of the impinging molecules is not related to the pre-impingement state of the molecules.

The physical space is divided into a certain number of regions, which are subdivided into computational cells. The dimensions of the cells must be such that the change in flow properties across each cell is small compared to the mean free path. The cell provides a convenient reference for the sampling of the macroscopic gas properties. The smallest unit of physical space is the subcell, where the collision partners are selected for the establishment of the collision rate. Time is advanced in discrete steps such that each step is small in comparison with the mean collision time, which is defined as the mean time between the successive collisions suffered by any particular molecule. A view of the computational domain is depicted in Figure 2. Only half of the body needs to be considered because of its symmetry. The computational domain is made large enough so that the upstream and side boundaries can be specified as freestream conditions. The flow at the downstream outflow boundary is predominantly supersonic and vacuum conditions are specified [11].

Numerical accuracy in DSMC method depends on the grid resolution chosen as well as the number of particles per computational cell. Both effects were investigated to determine the number of cells and the number of particles required to achieve grid independence solutions for the thermal nonequilibrium flow that arises near the leading edges. A discussion of both effects on the aerodynamic surface quantities is described in the appendix.

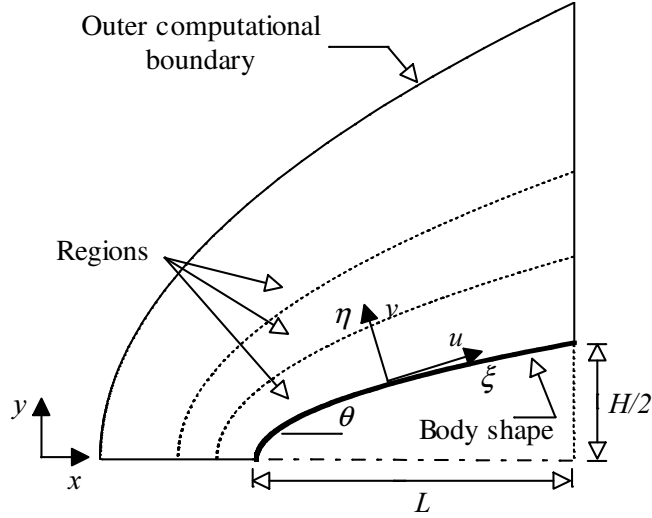


Figure 2: Schematic view of the computational domain.

The freestream and flow conditions used in the present calculations are those given by Bertin [14] and summarized in Table 2. The freestream velocity V_∞ is assumed to be constant at 2.9 Km/s, which corresponds to freestream Mach number $M_\infty = 10$. The wall temperature T_w is assumed constant at 880 K, chosen to be four times the freestream temperature. The overall Knudsen number is defined as the ratio of the molecular mean free path in the freestream gas to a characteristic dimension of the flowfield. In the present study, the characteristic dimension was defined as being the diameter of the circular cylinder. Therefore, the freestream Knudsen number corresponds to $Kn_\infty (= \lambda_\infty/2R) = 0.0903$. Finally, the freestream Reynolds number by unit meter Re_∞ is 17889.

Table 2: Freestream Conditions

Parameter		Value	Unit
Altitude		70	km
Temperature (T_∞)		220.0	K
Pressure (p_∞)		5.582	N/m ²
Density (ρ_∞)		8.753×10^{-5}	kg/m ³
Viscosity (μ_∞)		1.455×10^{-5}	Ns/m ²
Number density (n_∞)		1.8209×10^{21}	m ⁻³
Mean free path (λ_∞)		9.03×10^{-4}	m
Molecular weight		28.96	kg/kg mole
Molecular mass	O ₂	5.312×10^{-26}	kg
Molecular mass	N ₂	4.65×10^{-26}	kg
Molecular diameter	O ₂	4.01×10^{-10}	m
Molecular diameter	N ₂	4.11×10^{-10}	m
Mole fraction	O ₂	0.237	
Mole fraction	N ₂	0.763	

COMPUTATIONAL RESULTS AND DISCUSSION

Attention is now focused on the heat transfer calculations and on the drag coefficient obtained from the DSMC results. The simulations were performed, as mentioned above, for power law exponents of 1/4, 1/2, and 3/4. The present calculations correspond to freestream Mach number of 10, wall temperature of 880 K, and freestream conditions associated to an altitude of 70 Km.

The heat flux to the body is calculated by the net energy fluxes of the molecules impinging on the surface. A flux is regarded as positive if it is directed toward the surface. The heat flux q_w is related to the sum of the translational, rotational and vibrational energies of both incident and reflected molecules as defined by,

$$q_w = q_i + q_r = \sum_{j=1}^N \left\{ \left[\frac{1}{2} m_j c_j'^2 + e_{Rj} + e_{Vj} \right]_i + \left[\frac{1}{2} m_j c_j'^2 + e_{Rj} + e_{Vj} \right]_r \right\} \quad (4)$$

where N is the number of molecules colliding with the surface by unit time and unit area, m is the mass of the molecules, c' is the thermal velocity of the molecules, e_R and e_V stand for the rotational and vibrational energies, and subscripts i and r refer to incident and reflected molecules.

The heat flux q_w is based upon the gas-surface interaction model of fully accommodated, completely diffuse re-emission. This is the most common model assumed, even though it is well known that some degree of specular reflection and less than complete accommodation are more realistic assumptions [15].

The heat flux is normalized by $\frac{1}{2} \rho_\infty V_\infty^3$, which corresponds to 1.15 MW/m² for the freestream conditions, and presented in terms of heat transfer coefficient C_h . The effect of the power law exponent on the heat transfer coefficient C_h is illustrated in Figure 3(a) as a function of the dimensionless arc length s/λ_∞ measured from the stagnation point. It is seen that the heat transfer coefficient is sensitive to the power law exponent n near the stagnation point. It presents the maximum value in the stagnation point and drops off a short distance away of the leading edge as the power law exponent increases. Also, it is seen that the blunter the leading edge the lower the heat transfer coefficient in the stagnation region.

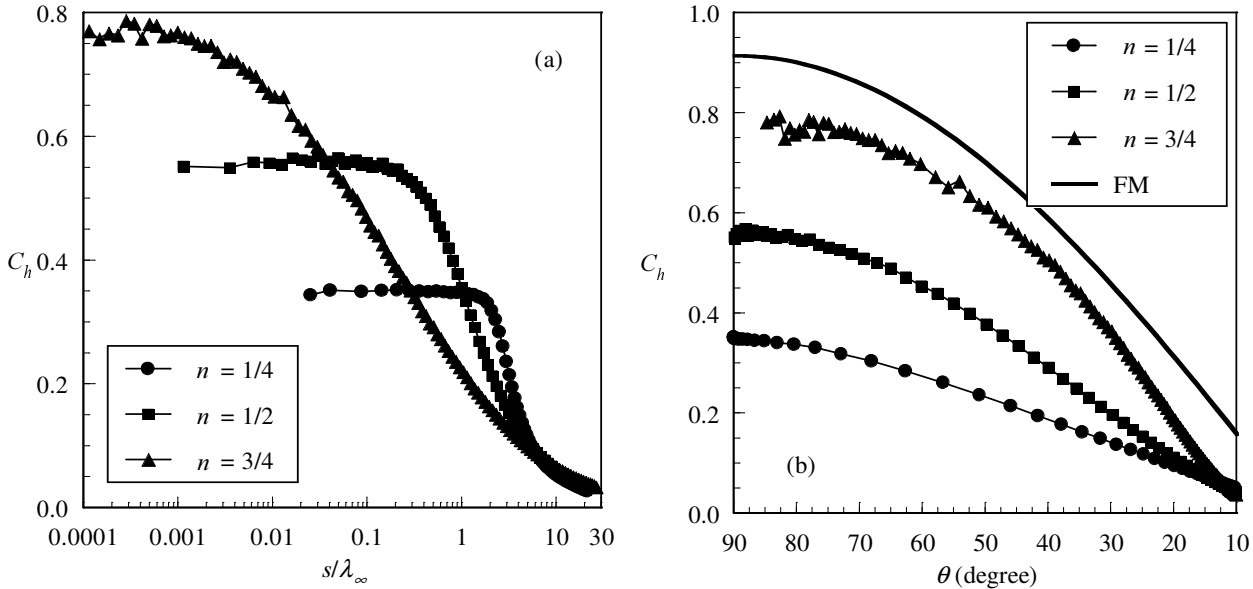


Figure 3: Heat transfer coefficient as a function of the (a) arc length and (b) of the body slope angle for power law exponents of 1/4, 1/2 and 3/4.

The leading edge geometry effect can also be seen by comparing the computational results with that predicted by free molecular flow (Bird [11]). Figure 3(b) displays this comparison for the heat transfer coefficient as a function of the body slope angle θ . These curves indicate that the heat transfer coefficient C_h increases as the leading edge becomes sharp, and approaches the free molecular value for the conditions investigated in this work.

Based on the computational results for the heat transfer coefficient (Figures 3(a-b)), the characteristic

of blunt bodies expressed by Eq. (1) seems to fail at the stagnation point, at least for power law bodies with $n \neq 1/2$. The heat flux is finite at the stagnation point for the leading edges investigated, even though the radii of curvature go to zero for the $n = 3/4$ case, and go to infinity for the $n = 1/4$ case.

In order to verify the dependence of the heat transfer coefficient C_h on the leading edge radius of curvature, the product $C_h \sqrt{R_c/\lambda_\infty}$, named here by function $K(n)$, is obtained from the DSMC results for the power law shapes investigated. Figures 4(a) (linear scaling) and 4(b) (log scaling) demonstrate this product as a function of the dimensionless arc length along the body surface. Interesting features can be drawn from Figures 4(a-b). In the vicinity of the stagnation point, the dependence of the heat transfer coefficient on the radius of curvature follows that predicted by the continuum flow, Eq. (1), for the power law shape with finite radius, $n = 1/2$ case. As would be expected, the dependence of the heat transfer coefficient on the radius of curvature in the stagnation region does not hold for power law leading edges defined by cases with $n \neq 1/2$. Furthermore, the function $K(n)$ tends to a constant value downstream to the stagnation region for the cases investigated. The constant value, which is a function of the power law exponent, is reached faster for the $n = 3/4$ than for the $n = 1/4$ case. As a result, it is seen that the heat transfer to the body is inversely proportional to the square root of the curvature radius of the power law shapes far from the stagnation region, independently of the power law exponent.

Referring to Figures 4(a-b), at first glance, one could conclude that power law shape defined by $n = 3/4$ gives lower value for heat flux at the stagnation point than $n = 1/2$ shape. Unfortunately, this does not hold as is demonstrated in Figure 3.

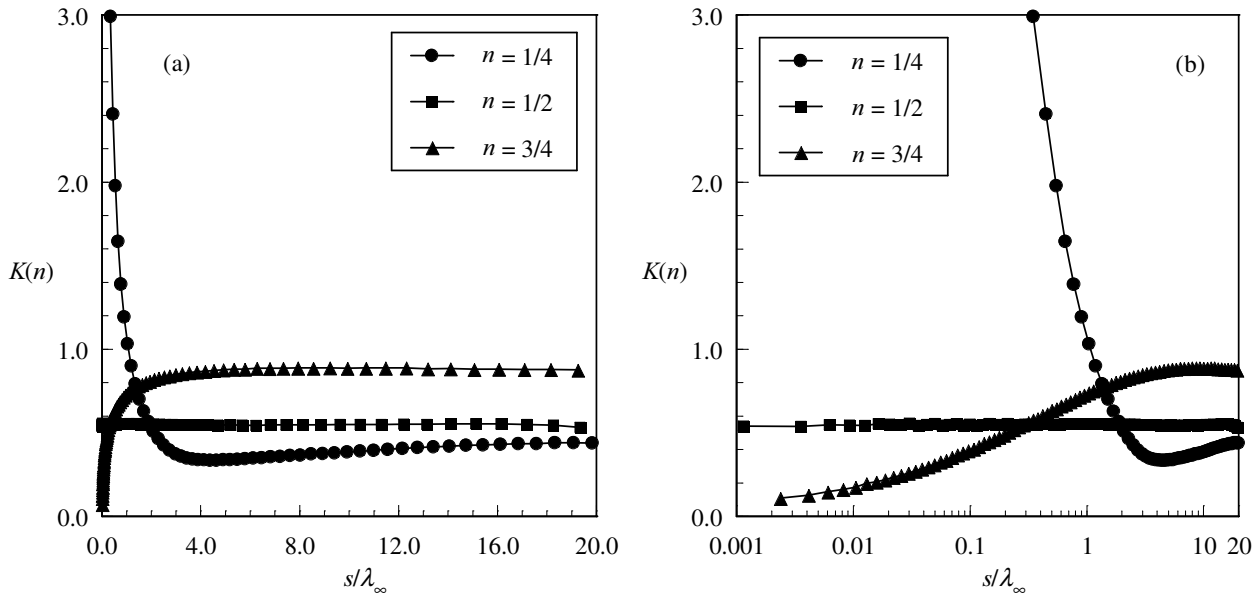


Figure 4: Heat transfer coefficient as a function of the arc length for power law exponents of 1/4, 1/2 and 3/4. (a) Linear scaling, and (b) log scaling.

The drag on a surface in a gas flow results from the interchange of momentum between the surface and the molecules colliding with the surface. The total drag is obtained by the integration of the pressure and shear stress distributions from the nose of the leading edge to the station L , which corresponds to the tangent point common to all of the body shapes (see Figure 1). It is important to mention that the values for the total drag presented in this section were obtained by assuming the shapes acting as leading edges. Therefore, no base pressure effects were taken into account in the calculations. Results are normalized by $\frac{1}{2}\rho_\infty V_\infty^2 H$ and presented as total drag coefficient C_d and its components of pressure drag coefficient and skin friction drag coefficient.

Figure 5(a) illustrates the total drag coefficient as a function of the power law exponent n . The

contributions of the pressure drag coefficient and the skin friction coefficient are also displayed in this Figure. For $n = 1/4$ case, the total drag coefficient is dominated by pressure drag, a characteristic of a blunt body. In contrast, for $n = 3/4$, the total drag coefficient is dominated by the skin friction drag, a characteristic of a sharp body. As the net effect on total drag depends on these opposite behaviors, appreciable changes are observed in the total drag coefficient for the power law exponent range investigated. As a reference, the total drag coefficient for the $n = 1/4$ case is around 24% higher than that for the $n = 3/4$ case.

Figure 6(b) displays the percentage of the skin friction drag and pressure drag on total drag. It is seen that for power law exponent of $1/4$, the shear forces account for 9% of the total drag forces on the leading edge, whereas for power law exponent of $3/4$, it accounts for 68%.

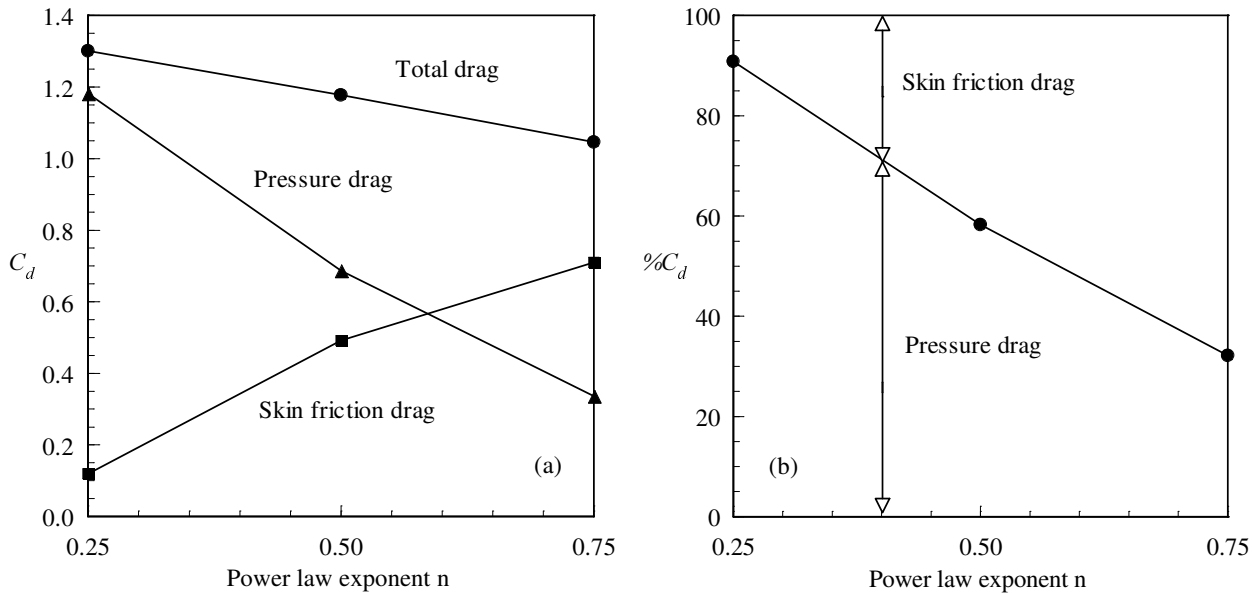


Figure 6: (a) Pressure and skin friction drag contributions on the total drag, and (b) the percentage of the pressure and skin friction drag as a function of the power law exponent n .

CONCLUDING REMARKS

Through the use of DSMC method, the heat flux to and drag acting on power law shapes have been investigated. The calculations provided information concerning the nature of the heat transfer coefficient and the total drag coefficient along the body surface resulting from variations in the body shape for the idealized situation of two-dimensional hypersonic rarefied flow. Results for power law exponents of $1/4$, $1/2$, and $3/4$ indicate that the heat flux approaches that one predicted by the free molecular flow as the power law shape becomes aerodynamically sharp, for the flow conditions considered. A substantial reduction of the aerodynamic heating at the stagnation point is observed as the power law exponent decreases. On the other hand, a power law exponent decrease is associated with a drag increase. Furthermore, the stagnation point heating for the power law shapes does not follow that one for classical blunt body in the vicinity of the leading edge for power law exponents different from $1/2$. Nevertheless, the heat transfer varies inversely with the square root of the radius of curvature far from the stagnation region.

APPENDIX

This section focuses on the analysis of the influence of the cell size and the number of particles per computational cell on the surface properties in order to achieve grid independence solutions. The effect of grid resolution on computed results is of particular interest for the present study since insufficient grid

resolution can reduce significantly the accuracy of the predicted aerodynamic heating and forces acting on the body surface. Hence, heat transfer, pressure and skin friction coefficients were used as the representative parameters for the grid sensitivity study. However, because of the reduced number of pages in the paper, the analysis will be shown only for heat transfer coefficient related to the $n = 1/2$ case.

The effect of altering the size of the computational cells is investigated for a series of three simulations with grids of 35 (coarse), 70 (standard) and 105 (fine) cells in the ξ -direction and 50 cells in the η -direction (see Figure 2). Each grid was made up of nonuniform cell spacing in both directions. The effect of changing the number of cells in the ξ -direction is illustrated in Figure A(a) as it impacts the calculated heat transfer coefficient. The comparison shows that the calculated results are rather insensitive to the range of cell spacing considered.

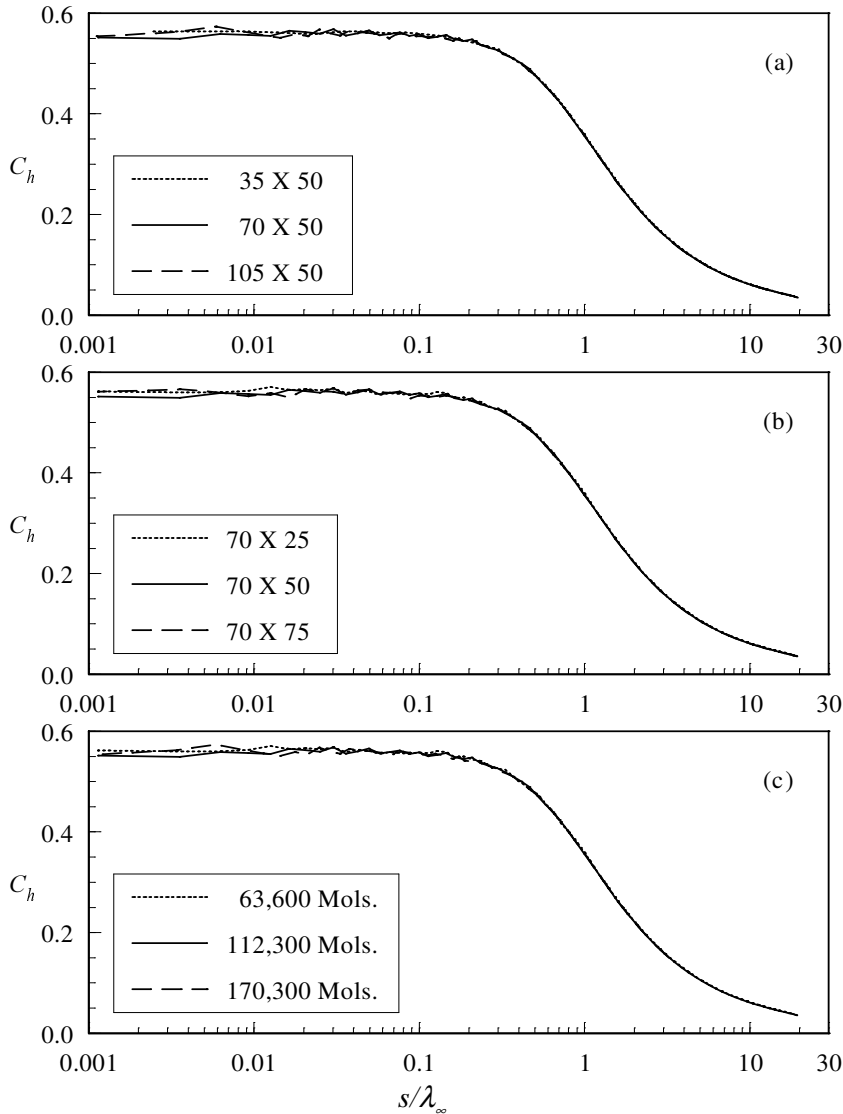


Figure A: Effect of altering the cell size (a) in the ξ -direction, (b) in the η -direction, and (c) in the number of molecules on heat transfer coefficient.

In analogous fashion, an examination was made in the η -direction. The sensitivity of the calculated results to cell size variations in the η -direction is displayed in Figure A(b) for heat transfer coefficient. In this Figure, a new series of three simulations with grid of 70 cells in the ξ -direction and 25 (coarse), 50

(standard) and 75 (fine) cells in the η -direction is compared. The cell spacing in both directions is again nonuniform. According to Figure A(b), the results for the three grids are approximately the same, indicating that the standard grid, 70 X 50 cells, is essentially grid independent. For the standard case, the cell size in the η -direction is always less than the local mean free path length in the vicinity of the surface.

A similar examination was made for the number of molecules. The sensitivity of the calculated results to number of molecule variations is demonstrated in Figure A(c) for heat transfer coefficient. The standard grid, 70 x 50 cells, corresponds to a total of 112,300 molecules. Two new cases using the same grid were investigated. These new cases correspond to, on average, 63,600 and 170,300 molecules in the entire computational domain. It is seen that the standard grid with a total of 112,300 molecules is enough for the computation of the aerodynamic surface quantities.

ACKNOWLEDGMENTS

The author is grateful to the High Performance Computer Center (NACAD-COPPE/UFRJ) at the Universidade Federal do Rio de Janeiro (Federal University of Rio de Janeiro) for use of the workstations.

REFERENCES

1. Mason, W. H., and Lee, J., 1994, Aerodynamically Blunt and Sharp Bodies, *J. of Spacecraft and Rockets*, **31(3)**, pp.378-382.
2. Sibulkin, M., 1952, Heat Transfer Near the Forward Stagnation Point of a Body of Revolution, *J. of Aeronautical Sciences*, **19(8)**, pp. 570-571.
3. Lees, L., 1956, Laminar Heat Transfer over Blunt-Nosed Bodies at Hypersonic Flight Speeds, *Jet Propulsion*, **26(4)**, pp. 259-269.
4. Romig, M., 1956, Stagnation Point Heat Transfer for Hypersonic Flow, *Jet Propulsion*, **26(12)**, pp. 1098-1101.
5. Fay, J. A., and Riddell, F. R., 1958, Theory of Stagnation Point Heat Transfer in Dissociated Air, *J. of Aeronautical Sciences*, **25(2)**, pp. 73-85.
6. Cohen, N. B., 1961, Boundary-Layer Similar Solutions and Correlation Equations for Laminar Heat-Transfer Distribution in Equilibrium Air at Velocities up to 41,000 feet per second, NASA TR R-118.
7. Sutton, K., and Graves, R. A. Jr., 1971, A General Stagnation-Point Convective-Heating Equation for Arbitrary Gas Mixtures, NASA TR R-376.
8. Zoby, E. V., Moss, N. J., and Sutton, K., 1981, Approximate Convective-Heating Equations for Hypersonic Flows, *J. of Spacecraft and Rockets*, **18(1)**, pp.64-70.
9. Zuppari, G., and Verde, G., 1998, Improved Fay-Riddell Procedure to Compute the Stagnation Point Heat Flux, *J. of Spacecraft and Rockets*, **35(3)**, pp. 403-405.
10. DeJarnette, F. R., Hamilton, H. H., Weilmuenster, K. J., and Cheatwood, F. M., 1987, A Review of some Approximate Methods Used in Aerodynamic Heating Analysis, *J. of Thermophysics and Heat Transfer*, **1(1)**, pp. 5-12.
11. Bird, G. A., 1994, *Molecular Gas Dynamics and the Direct Simulation of Gas Flows*, 1st edition, Oxford University Press, Oxford, England, UK.
12. Bird, G. A., 1988, Monte Carlo Simulation in an Engineering Context, *Progress in Astronautics and Aeronautics: Rarefied gas Dynamics*, ed. by Sam S. Fisher, AIAA New York, Vol. 74, part I, pp.239-255.
13. Borgnakke, C., and Larsen, P. S., 1975, Statistical Collision Model for Monte Carlo Simulation of Polyatomic Gas Mixture, *J of computational Physics*, **18**, pp.405-420.
14. Bertin, J. J., 1994, *Hypersonic Aerothermodynamics*, 1st edition, AIAA Education Series, Washington D.C..
15. Haas, B. L., and Fallavollita, M. A., 1994, Flow Resolution and Domain Influence in Rarefied Hypersonic Blunt-Body Flows, *J. of Thermophysics and Heat Transfer*, **8(4)**, pp.751-757.